Reconfigurable Spin-Wave Nonreciprocity Induced by Dipolar Interaction in a Coupled Ferromagnetic Bilayer

R.A. Gallardo,[1,2] T. Schneider,[3] A.K. Chaurasiya,[4] A. Oelschlägel,[3,5] S.S.P.K. Arekapudi,[6]
A. Roldán-Molina,[7] R. Hübner,[3] K. Lenz,[3] A. Barman,[4] J. Fassbender,[3,5] J. Lindner,[3] O. Hellwig[3,6,*]
and P. Landeros[1,2,†]

[1]*Departamento de Física, Universidad Técnica Federico Santa María, Avenida España 1680, Valparaíso, Chile*
[2]*Center for the Development of Nanoscience and Nanotechnology (CEDENNA), 917-0124 Santiago, Chile*
[3]*Institute of Ion Beam Physics and Materials Research, Helmholtz-Zentrum Dresden-Rossendorf, Bautzner Landstr. 400, 01328 Dresden, Germany*
[4]*Department of Condensed Matter Physics and Material Sciences, S. N. Bose National Centre for Basic Sciences, Block JD, Sec. III, Salt Lake, Kolkata 700106, India*
[5]*Institute of Materials Science, Technische Universität Dresden, 01062 Dresden, Germany*
[6]*Institute of Physics, Chemnitz University of Technology, 09126 Chemnitz, Germany*
[7]*Universidad de Aysén, Ovispo Vielmo 62, Coyhaique, Chile*

Frequency nonreciprocity of wave phenomena describes the situation where the wave dispersion depends on the sign of the wave vector, i.e., counterpropagating waves exhibit different wavelengths for the same frequency. Such behavior has recently been observed in heavy-metal–ferromagnetic interfaces with Dzyaloshinskii-Moriya coupling, and is also known for coupled magnetic bilayers, where the nonreciprocity is enhanced when the two layers are aligned antiparallel. Besides the conventional uses of spin waves, nonreciprocity adds further functionalities, such as its potential applications in communication technologies and logic operations. In the current paper, we thus examine the spin-wave nonreciprocity induced by dipolar interactions in a coupled bilayer consisting of two ferromagnetic layers separated by a nonmagnetic spacer. We derive an easy-to-use formula to estimate the frequency difference provided by the nonreciprocity, which allows one to choose an optimal system in order to maximize the effect. For small wave numbers, the nonreciprocity scales linearly, while for larger wave vectors the nonreciprocity behaves nonmonotonically, with a well-defined maximum. The study is carried out by means of analytical calculations that are complemented by micromagnetic simulations. Furthermore, we confirm our model by experimental investigation of the spin-wave dispersion in a prototype antiparallel-coupled bilayer system. Since the relative magnetic orientation can be controlled through a bias field, the magnon nonreciprocity can then be turned on and off, which lends an important functionality to the coupled ferromagnetic bilayers.

I. INTRODUCTION

The engineering of spin waves (SWs)—the elementary excitations in magnetic systems with coupled electron spins—in magnetic structures is attracting a lot of attention in the scientific community, motivated by applications based on the field of magnon spintronics [1], which also provides a rich playground to study the fundamental principles of magnetic wave phenomena [2–9]. Since SW frequencies can vary from GHz to THz and can be externally controlled by applying magnetic fields

or by designing the system architecture to create desired magnonic properties, devices for high-frequency applications and data processing are envisioned [10–17]. In the context of data processing, the nonreciprocity of spin waves, which can appear in the phase, amplitude, or frequency, has been presented as a powerful tool for possible applications in communication and logic devices [18–20]. Nonreciprocal phenomena have been the focus of studies on photonic and electronic structures as well, in which they have been found to enable fundamental operation modes in devices such as isolators, circulators, or gyrators [21,22]. Similarly, nonreciprocal magnon transport yields these key functionalities as well [18]. Consequently, achieving nonreciprocity in the spin-wave dispersion up to

---

a significant, ideally tunable, degree is of high relevance for magnon-based applications.

Spin-wave nonreciprocity has been known since the pioneering work of Damon and Eshbach [23], where it was predicted that the magnetization precession amplitude of the surface mode should be asymmetric with respect to the propagation direction. Such behavior is well known and has been experimentally measured by several groups [24–26]. However, the amplitude nonreciprocity itself does not imply nonreciprocity in frequency. In our current bilayer case, symmetry breaking along the thickness will induce a frequency shift of the two counterpropagating waves. Spin-wave frequency nonreciprocity has already been discussed for ferromagnetic (FM) films with different magnetic anisotropies at the surfaces [27–32] and for films with interband magnonic transitions [33]. It has, moreover, been theoretically and experimentally demonstrated that the interfacial Dzyaloshinskii-Moriya interaction (DMI) [34–37] induced in ultrathin FM layers capped with heavy-metal films noticeably influences the SW spectra, generating nonreciprocity in the dispersion [38–54]. Additionally, nonreciprocal properties can be introduced into FM materials by the intrinsic dipolar interactions. It has been reported that arrays of magnetic nanopillars coupled by dipolar interaction [55], ferromagnetic nanotubes [56], systems composed of a FM film exchange-coupled to a one-dimensional periodic structure [57,58], and antiferromagnetic trilayers [59,60] show SW nonreciprocity. Although the physical properties of magnetic multilayers have been extensively studied in past decades, the focus was put on the celebrated giant change of magnetoresistance with the relative magnetic orientation of adjacent FM layers [61–63]. Interestingly, early studies of double layers and multilayers by Brillouin light scattering (BLS) had already evidenced frequency nonreciprocity for antiparallel alignment of the magnetic layers [64–68], in agreement with theoretical work [18,69–73]. However, a theory with the potential of making specific predictions is so far still missing, which hinders establishing the advantages and/or disadvantages of specific systems in comparison with others.

In this paper, the spin-wave dynamics of a FM bilayer system is investigated using a theoretical model, micromagnetic simulations, and BLS experiments. By analyzing both the magnetic properties of each layer and their equilibrium configurations, optimal conditions for increasing the frequency nonreciprocity of counterpropagating SWs in the Damon-Eshbach configuration are predicted and then confirmed with computer simulations and BLS for a prototype permalloy/Ir/Co-Fe-B sample. An explicit expression is provided for the frequency shift Δf of two counterpropagating SWs. In the long-wavelength limit (small wave vector k), we find that the SW nonreciprocity scales linearly with k, so that an effective DMI constant of dipolar origin can be defined. At intermediate values

of k, there is a maximum in Δf that depends only on the thicknesses of the FM layers and the nonmagnetic spacer, while for larger k, Δf decreases exponentially. Thus, we demonstrate that the proposed bilayer systems exhibit remarkable properties as compared with the widely discussed heavy-metal–ferromagnetic ultrathin systems. In particular, in bilayer systems with antiparallel coupling, and in fundamental contrast to DMI-driven systems, the nonreciprocity can be notably larger for thicker FM layers also. This opens up the possibility to create reconfigurable nonreciprocal devices [18,74,75] by controlling the relative magnetic orientation between the coupled FM layers. In the proposed bilayer system, frequency nonreciprocity can be turned on and off simply by switching from antiparallel to parallel magnetization, without any rotation of the applied magnetic field. Such switching can even be controlled and conveniently achieved by applying, for example, spin-transfer or spin-orbit torques via a local critical current. Moreover, both states, parallel and antiparallel, are well known from applications of giant magnetoresistance (GMR) and tunnel magnetoresistance (TMR) and can be tuned to have excellent stability at remanence. Therefore, the bilayer has a remarkable advantage over other systems, such as DMI-driven systems, where reconfigurability can be achieved by rotating the magnetization either in-plane, from the Damon-Eshbach (DE) to the backward-volume configuration, or by tipping the magnetization out of the plane [41,45,46,52]. Also, in interfacial DMI systems there is a noticeable increment in magnetic damping due to the heavy metal, which is avoided when a coupled magnetic bilayer is used instead. Another advantage is that the bilayer system is compatible with standard deposition processes in the same manner as that in which GMR stacks are fabricated, and can be integrated into CMOS architectures.

II. THEORY AND SIMULATIONS

A schematic illustration of the bilayer system considered, composed of two interacting FM layers (1) and (2) with in-plane magnetization, is shown in Fig. 1. The two layers are allowed to exhibit different magnetic parameters and thicknesses d_1 and d_2, and s denotes the separation between them. The equilibrium magnetization of layer $v = 1, 2$ makes an angle φ_v with the z axis, which is chosen as the propagation direction of the SWs, with wave vector $\mathbf{k} = k\hat{z}$. As we shall see, the nonreciprocity is enhanced in the Damon-Eshbach configuration, particularly in the antiparallel state. Nonetheless, the theoretical approach accounts for the general case where the wave vector and magnetization may be oriented along arbitrary directions within the film plane, and moreover accounts for the highly relevant magnetostatic fields created by the dynamic magnetizations.
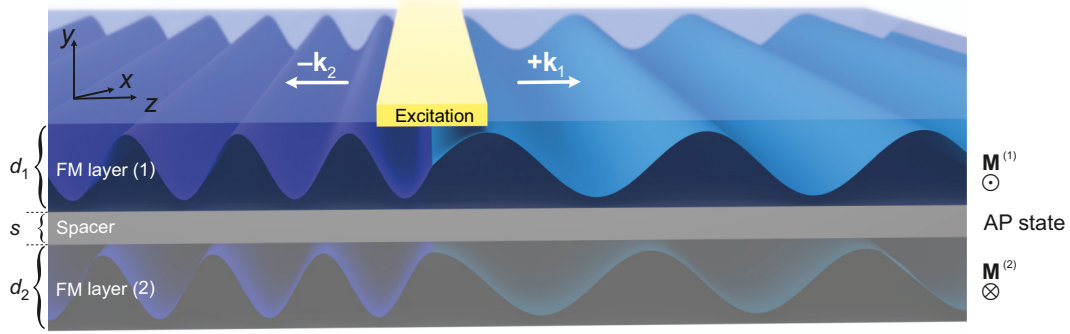
FIG. 1. Overview of the magnetic bilayer system. The static magnetization configuration is in the antiparallel (AP) state. A spin wave is excited below the yellow region, traveling along positive and negative wave vectors with different wavelengths as indicated by the different color of the waves.

A. Theory

The Landau–Lifshitz–Gilbert (LLG) equation is linearized and solved with the effective field contribution, as explained in the Supplemental Material [76]. For the symmetric case of two identical FM layers with the same thickness $d_1 = d_2 = d$, aligned along x but antiparallel to each other, an analytic formula for the SW dispersion relation for small external fields is derived and reads

$$f_{m_1}(k) = \frac{\gamma}{2\pi}\left\{g(k) + \sqrt{[p(k)-g(|k|)][q(k)-g(|k|)-2C_J]}\right\}, \quad (1)$$

$$f_{m_2}(k) = \frac{\gamma}{2\pi}\left\{-g(k) + \sqrt{[q(k)+g(|k|)][p(k)+g(|k|)-2C_J]}\right\}, \quad (2)$$

where $f_{m_1}(k)$ and $f_{m_2}(k)$ correspond to the two modes, namely the low and high frequency modes, of the bilayer system. In what follows, the mode analyzed will be the low-frequency one that corresponds to $f_{m_1}(k)$. The individual terms are defined by

$$g(k) = \mu_0 M_s \zeta(k)^2 e^{-|k|s} k\, d/2, \quad (3)$$

$$p(k) = \mu_0 H_u + \mu_0 M_s k^2 \lambda_{\text{ex}}^2 + \mu_0 M_s[1-\zeta(k)], \quad (4)$$

$$q(k) = \mu_0 H_u - \mu_0 H_s + \mu_0 M_s k^2 \lambda_{\text{ex}}^2 + \mu_0 M_s \zeta(k), \quad (5)$$

where

$$\zeta(k) = \frac{\sinh(kd/2)}{kd/2} e^{-|k|d/2}, \quad (6)$$

and $C_J = (J_{\text{bl}} - 2J_{\text{bq}})/(M_s d)$. Here, $J_{\text{bl}}/M_s d$ ($J_{\text{bq}}/M_s d$) is the bilinear (biquadratic) interlayer exchange field, $\mu_0 H_u$ is a possible uniaxial in-plane anisotropy field, M_s is the saturation magnetization, λ_{ex} is the exchange length, and

γ is the gyromagnetic ratio. Also, $\mu_0 H_s$ represents a surface uniaxial anisotropy field, which competes with the static dipolar field, allowing one to define an effective magnetization $\mu_0 M_{\text{eff}} = \mu_0 M_s - \mu_0 H_s$. The general case, assuming two different FM layers with different magnetic parameters, which is more complex, can be solved with the help of the eigenproblem presented in the Supplemental Material [76].

From Eqs. (1)–(3), it is clearly visible that it is the term $g(k)$ that introduces the nonreciprocity. Only this term changes sign as a function of the wave number k. All other terms, $p(k)$, $q(k)$, and $\zeta(k)$, are positive for both wave-vector directions, and $\zeta(k)$ is bounded by 1. Then, considering the limit of small wave numbers yields

$$f_{m_1}(k\to 0) = f_{m_1}(0) - \frac{\gamma\mu_0}{4\pi}M_s d\left(k + \frac{\gamma\mu_0}{2\pi}\frac{H_u}{f_{m_1}(0)}|k|\right) \quad (7)$$

for the low-frequency mode, while the high-frequency mode, $f_{m_2}(k)$, follows a similar behavior (not shown). Upon inspection, one may realize that the magnon dispersion relation for a bilayer with an antiparallel orientation of the two ferromagnetic layers in the limit of small k resembles the well-known asymmetric dispersion of ultrathin magnetic films with a DMI [41,42,52]. Indeed, the frequency shift becomes $\Delta f_{\text{AP}} \approx \mu_0 \gamma (M_s d/2\pi)k$, which allows one to introduce an effective Dzyaloshinskii-Moriya constant, since the frequency shift in heavy-metal–ferromagnetic interfaces follows the same linear behavior with k. Thus, this effective constant induced in the system is given by $D^{\text{dip}} = \mu_0 M_s^2 d/4$. Due to the dipolar nature of the nonreciprocity induced in the system, the effective constant increases linearly with thickness and quadratically with the saturation magnetization. Despite the simplicity of D^{dip}, this expression is very practical and useful, as it provides the relevant magnetic parameters for optimizing the nonreciprocal system in order

to reach the desired properties for application purposes, where the nonreciprocity turns out to be relevant for operations in communication and logic devices [1,13]. Also, it allows one to identify if a bilayer is able to emulate a heavy-metal–ferromagnet system with respect to its nonreciprocal SW propagation. For instance, in bilayers of the heavy-metal–ferromagnet type, it has been found that the Dzyaloshinskii-Moriya constant D^{DM} is around 0.7 mJ/m^2 for a ferromagnet of thickness 1.6 nm [46]. Here, we can show that similar properties (i.e., $D^{DM} = D^{dip}$) can be reached for the same thickness of the ferromagnet (1.6 nm) if a saturation magnetization of $M_s = 1190$ kA/m is used. To further increase D^{DM}, it is possible to decrease the film thickness to less than 1 nm [48], which is analogous to increasing D^{dip} by increasing the thicknesses of both FM layers. This, added to the wide versatility of our system, allows us to establish that a ferromagnetic bilayer is an excellent candidate for nonreciprocal magnonic devices, which, due to its simplicity and scalability, outperforms other systems proposed for corresponding applications in magnon-based data processing, where, for instance, the control of nonreciprocity allows the creation of unidirectional caustic spin waves [77] that are relevant for the suppression of cross-interference between devices within a magnonic circuit [57].

In the extended-k regime, we obtain further from Eqs. (1) and (2) the following analytical expression for Δf_{AP} for two counterpropagating spin waves:

$$\Delta f_{AP} = \frac{2\gamma}{\pi} \mu_0 M_s \sinh^2\left(\frac{kd}{2}\right) \frac{e^{-|k|(d+s)}}{kd}. \quad (8)$$

Note that Eq. (8) is valid for the modes $f_{m_1}(k)$ and $f_{m_2}(k)$ in such a way that we predict that both modes show asymmetric dispersion with the same magnitude of frequency shift. Equation (8) shows that interlayer exchange fields are not required for generating nonreciprocity, neither for small nor for large wave vectors. This demonstrates that the effect results solely from the dynamic dipolar interaction. Interlayer exchange coupling may, however, be used to (i) stabilize the AP alignment and (ii) influence the accessible frequency range.

B. Micromagnetic simulations

To validate the results of the theory, micromagnetic simulations are performed using the GPU-accelerated code MuMax3 [78]. For this, a long magnetic bilayer stripe with length $l = 20$ μm and width $w = 80$ nm is considered. To mimic the thin magnetic film, periodic boundary conditions are applied along the x and z directions. The material parameters are chosen in accordance with those mentioned above for the two systems, S_I and S_{II}. Using

$$\mathbf{h} = \tilde{h} \frac{\sin(k_0 z)}{k_0 z} \frac{\sin(2\pi f_0 t)}{2\pi f_0 t} \hat{y} \quad (9)$$

as an external rf-field source, the spin waves are excited with a sinc pulse in space with a cutoff wavelength $\lambda_0 = 2\pi/k_0 = 9.77$ nm, and in time with a cutoff frequency $f_0 = 50$ GHz. The coordinate system is based on the global coordinate system given in Fig. 1. To reconstruct the SW dispersion relation, the magnetization configuration is stored every 10 ps for 12.5 ns and subsequently Fourier transformed in 2D. Additionally, simulations of the hysteresis loops for in-plane and out-of-plane applied fields are performed. In this context, the total energy and the torque are subsequently minimized stepwise at varying applied-field values.

III. EXPERIMENTAL DETAILS

A. Sample preparation

A Ta(5 nm)/Co$_{40}$Fe$_{40}$B$_{20}$(5.7 nm)/Ir(0.6 nm)/Ni$_{81}$Fe$_{19}$(6.7 nm)/Ta cap layer stack is prepared on thermally oxidized Si substrates by magnetron sputtering in an Ar partial pressure of 0.35 Pa (2.62 mTorr) at room temperature. The deposition rates of each individual material are precalibrated by x-ray reflectivity (XRR). An underlayer of Ta (4 nm) is used to improve the adhesion. Ferromagnetic Co-Fe-B and Ni-Fe layers are deposited from alloy targets with compositions of Co$_{40}$Fe$_{40}$B$_{20}$ and Ni$_{81}$Fe$_{19}$ (in at.%), respectively (at a deposition rate of 0.3 Å/s). The ferromagnets are separated by a (nonmagnetic) Ir spacer layer to achieve antiferromagnetic alignment at zero field (via Ruderman–Kittel–Kasuya–Yoshida (RKKY) coupling). A Ta cap layer is used to provide an oxidation barrier.

B. BLS measurements

To investigate the spin-wave nonreciprocity, BLS measurements are performed in the DE geometry, i.e., by applying a bias magnetic field in the sample plane but perpendicular to the plane of incidence of the laser beam. This allows for probing the spin waves propagating along the in-plane direction perpendicular to the applied field, i.e., in the DE geometry, where the nonreciprocity in the spin-wave frequency is maximal at room temperature. BLS relies on an inelastic light-scattering process due to the interaction of the incident photons with magnons. The conventional 180° backscattered geometry is used along with the provision of wave-vector selectivity to investigate the spin-wave dispersion relation [79,80]. Monochromatic light (wavelength $\lambda = 532$ nm and power $P = 65$ mW) from a solid-state laser is focused on the sample surface. In the light-scattering process, the total momentum is conserved in the plane of the thin film. As a result, the Stokes (anti-Stokes) peaks in the BLS spectra correspond to the creation (annihilation) of magnons with momentum $k = 4\pi/\lambda \sin\theta$, where λ is the wavelength of the incident laser beam and θ refers to the angle of incidence of the

laser. Cross-polarizations between the incident and scattered beams are adopted in order to eliminate any phonon contribution to the scattered light, and only the magnon contribution is measured. Subsequently, the frequencies of the scattered light are analyzed using a Sandercock-type six-pass tandem Fabry-Pérot interferometer from JRS Scientific Instruments [81]. To get well-defined BLS spectra for the larger incidence angles, the spectra are obtained after counting photons for several hours. Because of the low frequency in the AP-coupled region, a free spectral range (FSR) of 30 GHz (20 GHz) for higher (lower) wavevectors and a 2^{10}-channel multichannel analyzer are used during the BLS measurement. The frequency resolution is determined by estimating FSR/$2^{10} \approx 0.05$ GHz (0.02 GHz) for higher (lower) wave vectors for the Stokes and anti-Stokes peaks of the BLS spectra. The sample magnetization is first saturated by applying a high enough magnetic field of -140 mT followed by reducing the field slowly to the bias magnetic field $\mu_0 H$, and BLS spectra are measured at that field for different values of the wave vector. The maximum value of the wave vector in our experiment is 20.4 rad/μm and the resolution is 2.06 rad/μm. For the first few wave vectors, the Stokes and anti-Stokes peaks merge with the tail of the elastic peaks and cannot be resolved; hence, we present the BLS spectra from $k = 6.1$ rad/μm. The nonreciprocity in the spin-wave frequency (Δf) is calculated by taking the difference between the anti-Stokes and Stokes peaks observed in the BLS spectra. Note that the BLS measurements are performed

in the conventional way, i.e., by investigating thermally excited spin waves. The effect on the frequency nonreciprocity, however, relies solely on the dispersion of the system and is thus not influenced by the exact method of spin-wave excitation.

IV. RESULTS AND DISCUSSION

To illustrate the main findings of the paper, permalloy (Py) and cobalt (Co) layers are first considered. For Py [assumed as layer (1)], a saturation magnetization $M_s^{(1)} = 658$ kA/m and an exchange length $\lambda_{ex}^{(1)} = 5.47$ nm are used, while for Co [layer (2)] the saturation magnetization is $M_s^{(2)} = 1150$ kA/m and $\lambda_{ex}^{(2)} = 5.88$ nm. Also, the gyromagnetic ratio is $\gamma = 1.7587 \times 10^{11}$ rad/T s, for simplicity assumed to be the same for both layers. Two kinds of bilayer configurations are addressed, a Py/Py bilayer referred to as S_I, and a Co/Py bilayer denoted by S_{II}, for which a uniaxial anisotropy field of $\mu_0 H_u^{(2)} = 69.6$ mT is assumed because of the hexagonal Co layer.

In order to induce an AP alignment between the two FM layers, we introduce an $s = 1$ nm thick spacer, leading to an interlayer exchange coupling constant of $J = -1.5$ mJ/m^2. The spin-wave dispersion relations calculated for different thicknesses of the FM layers for systems S_I and S_{II} are shown in Figs. 2(a) and 2(c). Here, the frequency of the counterpropagating SWs is calculated as a function of the wave vector k for AP magnetization. Micromagnetic simulations are performed and are shown
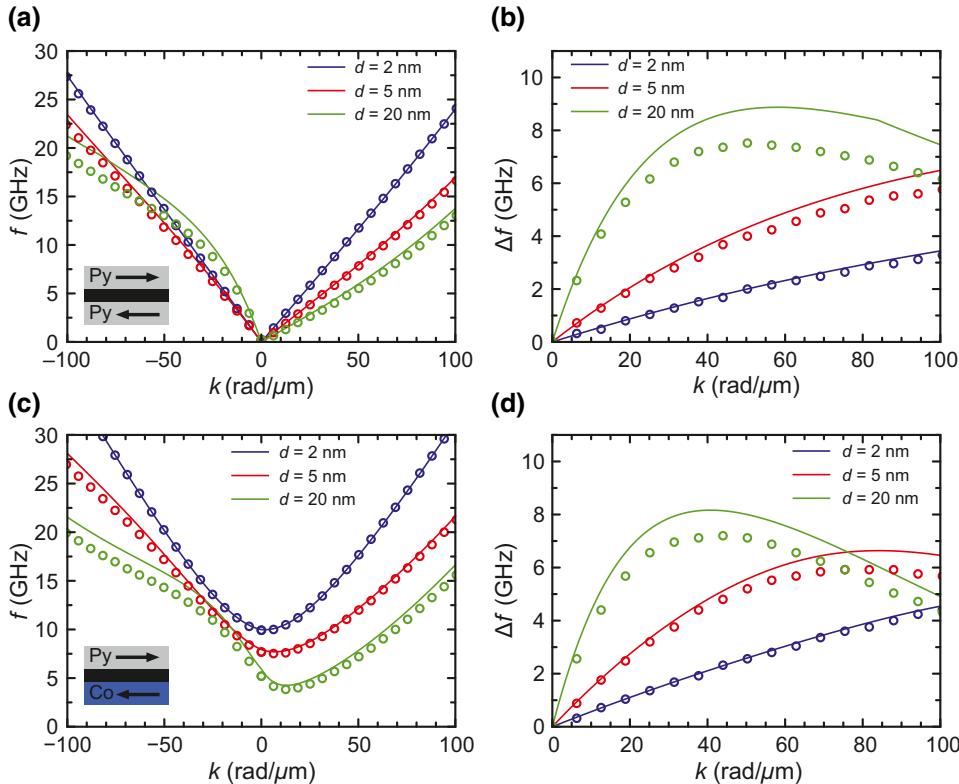
FIG. 2. Nonreciprocal magnon spectrum for coupled ferromagnetic bilayers. (a) Nonreciprocal spin-wave dispersion relation for the Py/Py system S_I and (c) for the Py/Co system S_{II}. (b),(d) Corresponding frequency shift Δf of two counterpropagating spin waves as a function of the wave number, for the case of antiparallel equilibrium states of the bilayers. In all plots, the open symbols show the results of the micromagnetic simulation and the solid lines depict the theory. The material parameters are given in the main text.

by the open symbols. The main deviation between theory and simulation occurs for large wave vectors, which corresponds to wavelengths of the same order of magnitude as the film thickness, so that the nonhomogeneous profile of the dynamic magnetization through the thickness will start to have a significant influence on the mode frequencies. In effect, the profile will tend to lower the nonreciprocity, so that the frequencies of the micromagnetic simulation are lower than those predicted by theory. In case of the non-symmetric system S_{II}, the deviation for large thicknesses occurs already at $k = 0$, because of the strong breaking of symmetry of the effective field due to the two layers having different magnetic parameters.

Our calculations and simulations for S_I in the case of parallel orientation of the two magnetizations yield a fully reciprocal dispersion. We note, however, that this is not the case for the asymmetric system S_{II}, for which a small non-reciprocity of about 0.6 GHz (at $k = 20$ rad/μm) remains even in the P case. Nonetheless, in both cases the nonreciprocity for antiparallel alignment by far exceeds that for parallel alignment, so that via switching between these two configurations the nonreciprocal behavior of spin waves can be turned on and off. This, in turn, allows for fabricating a nonreciprocal magnonic device that relies solely on the dynamic coupling of the spin waves in the FM bilayer.

In order to understand the physical mechanisms behind the large enhancement of the spin-wave nonreciprocity, the dynamic dipolar stray fields outside and inside the FM films are carefully analyzed. Figures 3(a) and 3(b) depict these fields created by the magnetic charges in the bilayer system for the AP state, where the large arrows represent the orientation of the dynamic magnetization. The main feature of these configurations is that the relative orientations of the dynamic stray field and the dynamic

magnetization depend on the static magnetization alignment and the wave number k. Therefore, the dynamic dipolar-interaction energy density $\epsilon_d = -(\mu_0/2)\mathbf{m} \cdot \mathbf{h}^{\text{stray}}$ differs between the cases presented. Here, the distribution of the stray field $\mathbf{h}^{\text{stray}}$ and the dynamic magnetizations for $k > 0$ and $k < 0$ are depicted in Fig. 3. In the AP state with $k > 0$ [Fig. 3(a)], the stray fields and the dynamic magnetizations are always parallel, in such a way that ϵ_d becomes small. Thus, this frequency represents a state of low energy that appears only in the AP configuration. In the configuration shown in Fig. 3(b) ($k < 0$), the stray fields are always opposite to the out-of-plane dynamic magnetization, inducing a higher ϵ_d as compared with the case presented in Fig. 3(a), notably increasing the SW frequencies, and therefore introducing nonreciprocity into the system.

In strong contrast to the DMI previously used, the non-reciprocity effects presented here are strongly tunable by the FM-layer thickness d, which also affects the maximum frequency difference. Furthermore, in the case of system S_I, it is easy to see that in the limits $d \to 0$ and $d \to \infty$ this frequency asymmetry becomes zero and, thus, there is a particular wave vector for which Δf_{AP} is maximum, which can be determined from the relation $\tanh(k^*d/2) = k^*d/[1 + k^*(d + s)]$. Consequently, only the geometrical parameters d and s determine the wave number k^*, for which the largest nonreciprocity is expected. Moreover, it is noted that the maximum frequency shift $\Delta f_{\text{AP}}(k^*)$ decays exponentially with the separation of the layers s and increases with the layer thickness d, due to the dipolar nature of the induced nonreciprocity.

To further validate the theory presented, BLS experiments are performed [6,28]. Three representative Brillouin light-scattering spectra for DE spin waves recorded at
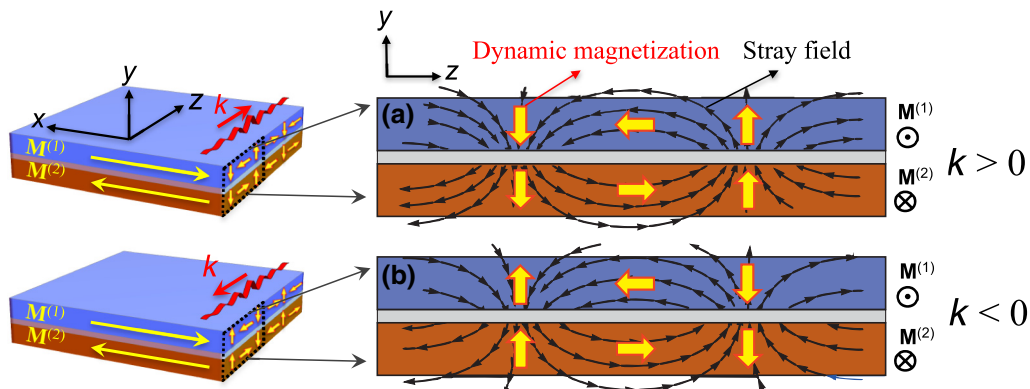

FIG. 3. Dynamic stray fields induced by the surface and volumetric magnetic charges in a ferromagnetic bilayer. The large arrows depict the orientation of the dynamic magnetization, while the static magnetizations point along the $\pm x$ directions. The distributions of dynamic magnetizations and stray fields are shown in (a) for $k > 0$ and (b) for $k < 0$, for an antiparallel equilibrium state. In agreement with Fig. 2, the lower-energy state is obtained for $k > 0$, shown in (a), where the dynamic magnetization and stray field are almost parallel.

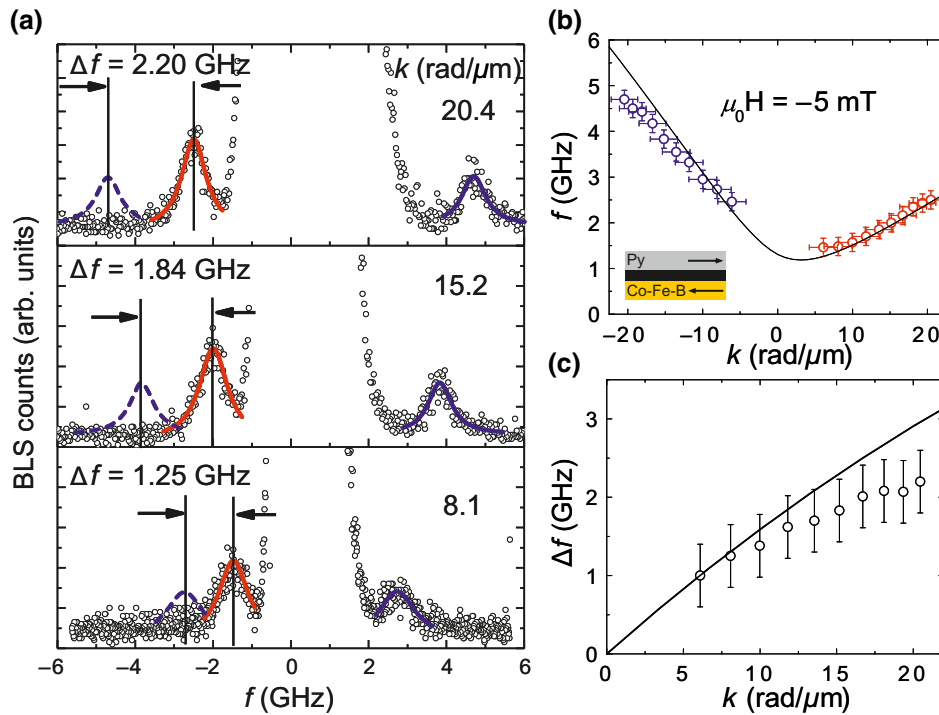FIG. 4.   Representative Brillouin light-scattering spectra for Damon-Eshbach spin waves recorded at an external applied field $\mu_0 H = -5$ mT in a $Co_{40}Fe_{40}B_{20}$(5.7 nm)/Ir(0.6 nm)/$Ni_{81}Fe_{19}$(6.7 nm) bilayer sample for two counterpropagating directions. The spectra correspond to a specific wave vector k as given in each panel. The open symbols are the experimental data points, whereas the solid curves (red and blue) are fits using a Lorentzian function. To show the frequency asymmetry (Δf), the mirror curve of the anti-Stokes peak (blue dotted curve) is superimposed. (b) Asymmetric spin-wave dispersion relation measured at $\mu_0 H = -5$ mT (in the antiferromagnetically coupled region). (c) Variation of Δf as a function of k. The solid lines in (b) and (c) correspond to analytical calculations. Results for the parallel state are shown in the Supplemental Material [76].

selected wave numbers under an in-plane bias magnetic field ($\mu_0 H = -5$ mT) are shown in Fig. 4(a). According to vibrating-sample magnetometry (with a conventional VSM) and SQUID-VSM loops, as shown in the Supplemental Material [76], this corresponds to the antiferromagnetically coupled region for the $Co_{40}Fe_{40}B_{20}$(5.7 nm)/Ir(0.6 nm)/$Ni_{81}Fe_{19}$(6.7 nm) sample investigated, where the thicknesses are estimated from transmission electron microscopy (TEM) measurements [76]. In order to estimate the frequency difference Δf between the counterpropagating spin waves (anti-Stokes and Stokes peaks), the mirror curve of the anti-Stokes peak is shown by a blue dotted curve for each spectrum. It is evident that Δf increases with increasing wave number. The value of Δf attains a maximum of 2.20 GHz at $k = 20.4$ rad/μm. Figure 4(b) shows the spin-wave dispersion relation measured at $\mu_0 H = -5$ mT. The dispersion relation is asymmetric with respect to the two oppositely propagating spin waves. Shown in Fig. 4(c) is the variation of Δf as a function of k for the AP state.

In order to fit the theoretical model to the experimental data, all the material parameters, besides the exchange constant, are determined experimentally. Ferromagnetic resonance (FMR) experiments are carried out to measure

all magnetic properties of the bilayer, such as the effective magnetization $\mu_0 M_{eff}$, the bilinear (biquadratic) interlayer exchange coupling constant J_{bl} (J_{bq}), and the anisotropy field $\mu_0 H_u$. As already discussed above, both the spacer thickness s and the FM-layer thicknesses d are crucial parameters for describing the nonreciprocity. These geometric parameters are determined by TEM. The experimentally determined material parameters are listed in Table I, and further details are provided in the Supplemental Material [76]. The agreement between the theory and the BLS experiments is good. In Fig. 4(b), it is visible that the positive wave numbers fit almost perfectly. However, for negative wave numbers the agreement is somewhat less perfect. To exclude the possibility that the material parameters cause this effect, the spin-wave dispersion for the parallel alignment was also measured. The results are shown in the Supplemental Material [76]. For the parallel case, the agreement is almost perfect. The deviation in the branch at negative k with higher group velocity may be related to the fact that in our system the in-plane anisotropy is rather weak (about a millitesla), so that some small tilting of the two ferromagnetic layers away from the AP alignment is not unlikely, due to a nonvanishing biquadratic coupling contribution. As shown

TABLE I. Experimentally determined material parameters. The magnetic properties are determined by FMR, SQUID, and conventional VSM. The layer thicknesses and the spacer thickness are determined by cross-section TEM.

	d (nm)	$\mu_0 M_{\mathrm{eff}}$ (mT)	$\mu_0 H_u$ (mT)	J_{bl} (mJ/m^2)	J_{bq} (mJ/m^2)	s (nm)
$Ni_{81}Fe_{19}$	6.7	942.5	4.0	−0.195	−0.044	0.6
$Co_{40}Fe_{40}B_{20}$	5.7	1442.9	0.0			

in the Supplemental Material [76], this scenario is confirmed by magnetometry data. In any case, such a small misalignment would lead to a reduction in the nonreciprocity, in particular for higher wave-vector values. A tilt angle of $25°$ would lead to a reduction in the nonreciprocity of approximately 50%.

V. CONCLUSIONS

The dynamic magnetic properties of a coupled ferromagnetic bilayer system are studied. By means of a spin-wave theory, micromagnetic simulations, and Brillouin light-scattering measurements, it is demonstrated that the dipolar interaction between the FM layers produced by the dynamic magnetizations is a notable source of nonreciprocity in the spin-wave frequency, with a remarkable property of reconfigurability that relies on control of the relative magnetic orientation of the interacting FM layers. In such bilayer structures, we can have in-plane remanent stable states with a parallel as well as an antiparallel configuration, as is well known from GMR and TMR applications. Therefore, one can reconfigure the bilayer system reliably into a reciprocal and a nonreciprocal device just by the magnetic-field history or, alternatively, by applying a local torque to one of the layers via a critical current density. The change from nonreciprocal to reciprocal spin waves is more difficult to obtain by switching the magnetization by $90°$ in the plane or $90°$ out of the plane, as required in other nonreciprocal systems. Also, in the small-wave-vector limit, we show that the bilayer system can emulate the nonreciprocity produced by the Dzyaloshinskii-Moriya interaction in FM–heavy-metal stacks, even for ultrathin ferromagnetic films. Thus, the bilayer system exhibits the ability to mimic the extensively studied dynamic properties of FM–heavy-metal layers and, at the same time, presents an easy way to control the magnitude of the nonreciprocity by means of the geometry and the equilibrium configuration. These findings open up alternative routes for the creation of nanoscale nonreciprocal magnonic devices and motivate a deeper study of this type of system, in order to optimize its design according to the desired application requirements.

[1] A. V. Chumak, V. I. Vasyuchka, A. A. Serga, and B. Hillebrands, Magnon spintronics, Nat. Phys. **11**, 453 (2015).

[2] G. Gubbiotti, S. Tacchi, G. Carlotti, N. Singh, S. Goolaup, A. O. Adeyeye, and M. Kostylev, Collective spin modes in monodimensional magnonic crystals consisting of dipolarly coupled nanowires, Appl. Phys. Lett. **90**, 092503 (2007).

[3] K.-S. Lee, D.-S. Han, and S.-K. Kim, Physical Origin and Generic Control of Magnonic Band Gaps of Dipole-exchange Spin Waves in Width-modulated Nanostrip Waveguides, Phys. Rev. Lett. **102**, 127202 (2009).

[4] S. Neusser and D. Grundler, Magnonics: Spin waves on the nanoscale, Adv. Mat. **21**, 2927 (2009).

[5] A. A. Serga, A. V. Chumak, and B. Hillebrands, YIG magnonics, J. Phys. D: Appl. Phys. **43**, 264002 (2010).

[6] G. Gubbiotti, S. Tacchi, M. Madami, G. Carlotti, A. O. Adeyeye, and M. Kostylev, Brillouin light scattering studies of planar metallic magnonic crystals, J. Phys. D: Appl. Phys. **43**, 264003 (2010).

[7] Z. K. Wang, V. L. Zhang, H. S. Lim, S. C. Ng, M. H. Kuok, S. Jain, and A. O. Adeyeye, Nanostructured magnonic crystals with size-tunable bandgaps, ACS Nano **4**, 643 (2010).

[8] J. Ding, M. Kostylev, and A. O. Adeyeye, Magnetic hysteresis of dynamic response of one-dimensional magnonic crystals consisting of homogenous and alternating width nanowires observed with broadband ferromagnetic resonance, Phys. Rev. B **84**, 054425 (2011).

[9] S. Tacchi, G. Duerr, J. W. Klos, M. Madami, S. Neusser, G. Gubbiotti, G. Carlotti, M. Krawczyk, and D. Grundler, Forbidden Band Gaps in the Spin-wave Spectrum of a Two-dimensional Bicomponent Magnonic Crystal, Phys. Rev. Lett. **109**, 137202 (2012).

[10] S.-K. Kim, K.-S. Lee, and D.-S. Han, A gigahertz-range spin-wave filter composed of width-modulated nanostrip magnonic-crystal waveguides, Appl. Phys. Lett. **95,** 082507 (2009).

[11] A. V. Chumak, V. I. Vasyuchka, A. A. Serga, M. P. Kostylev, V. S. Tiberkevich, and B. Hillebrands, Storage-recovery Phenomenon in Magnonic Crystal, Phys. Rev. Lett. **108,** 257207 (2012).

[12] H. Yu, G. Duerr, R. Huber, M. Bahr, T. Schwarze, F. Brandl, and D. Grundler, Omnidirectional spin-wave nanograting coupler, Nat. Commun. **4,** 2702 (2013).

[13] M. Jamali, J. H. Kwon, S.-M. Seo, K.-J. Lee, and H. Yang, Spin wave nonreciprocity for logic device applications, Sci. Rep. **3,** 3160 (2013).

[14] A. V. Chumak, A. A. Serga, and B. Hillebrands, Magnon transistor for all-magnon data processing, Nat. Commun. **5,** 4700 (2014).

[15] T. Brächer, F. Heussner, P. Pirro, T. Meyer, T. Fischer, M. Geilen, B. Heinz, B. Lägel, A. A. Serga, and B. Hillebrands, Phase-to-intensity conversion of magnonic spin currents and application to the design of a majority gate, Sci. Rep. **6,** 38235 (2016).

[16] B. Rana and Y. C. Otani, Voltage-controlled Reconfigurable Spin-wave Nanochannels and Logic Devices, Phys. Rev. Appl. **9,** 014033 (2018).

[17] A. V. Sadovnikov, V. A. Gubanov, S. E. Sheshukova, Yu P. Sharaevskii, and S. A. Nikitov, Spin-wave Drop Filter Based on Asymmetric Side-coupled Magnonic Crystals, Phys. Rev. Appl. **9,** 051002 (2018).

[18] R. E. Camley, Nonreciprocal surface waves, Surf. Sci. Rep. **7,** 103 (1987).

[19] J. Lan, W. Yu, R. Wu, and J. Xiao, Spin-wave Diode, Phys. Rev. X **5,** 041049 (2015).

[20] X. S. Wang, H. W. Zhang, and X. R. Wang, Topological Magnonics: A Paradigm for Spin-wave Manipulation and Device Design, Phys. Rev. Appl. **9,** 024029 (2018).

[21] N. Reiskarimian and H. Krishnaswamy, Magnetic-free non-reciprocity based on staggered commutation, Nat. Commun. **7,** 11217 (2016).

[22] D. L. Sounas and A. Alù, Non-reciprocal photonics based on time modulation, Nat. Photonics **11,** 774 (2017).

[23] R. W. Damon and J. R. Eshbach, Magnetostatic modes of a ferromagnet slab, J. Phys. Chem. Solids **19,** 308 (1961).

[24] L. K. Brundle and N. J. Freedman, Magnetostatic surface waves on a y.i.g. slab, Electron. Lett. **4,** 132 (1968).

[25] T. Wolfram and R. E. DeWames, Surface dynamics of magnetic materials, Prog. Surf. Sci. **2,** 233 (1972).

[26] V. E. Demidov, M. P. Kostylev, K. Rott, P. Krzysteczko, G. Reiss, and S. O. Demokritov, Excitation of microwaveguide modes by a stripe antenna, Appl. Phys. Lett. **95,** 112509 (2009).

[27] B. Hillebrands, Spin-wave calculations for multilayered structures, Phys. Rev. B **41,** 530 (1990).

[28] B. Hillebrands, *Light Scattering in Solids VII: Crystal-field and Magnetic Excitations* (Springer, Berlin, Heidelberg, 2000), p. 174.

[29] P. K. Amiri, B. Rejaei, M. Vroubel, and Y. Zhuang, Non-reciprocal spin wave spectroscopy of thin Ni—Fe stripes, Appl. Phys. Lett. **91,** 062502 (2007).

[30] M. Mruczkiewicz, M. Krawczyk, G. Gubbiotti, S. Tacchi, Yu A. Filimonov, D. V. Kalyabin, I. V. Lisenkov, and S. A. Nikitov, Nonreciprocity of spin waves in metallized magnonic crystal, New J. Phys. **15,** 113023 (2013).

[31] M. Mruczkiewicz, E. S. Pavlov, S. L. Vysotsky, M. Krawczyk, Yu A. Filimonov, and S. A. Nikitov, Observation of magnonic band gaps in magnonic crystals with nonreciprocal dispersion relation, Phys. Rev. B **90,** 174416 (2014).

[32] O. Gladii, M. Haidar, Y. Henry, M. Kostylev, and M. Bailleul, Frequency nonreciprocity of surface spin wave in permalloy thin films, Phys. Rev. B **93,** 054430 (2016).

[33] K. Di, H. S. Lim, V. L. Zhang, S. C. Ng, and M. H. Kuok, Spin-wave nonreciprocity based on interband magnonic transitions, Appl. Phys. Lett. **103,** 132401 (2013).

[34] I. Dzyaloshinsky, A thermodynamic theory of "weak" ferromagnetism of antiferromagnetics, J. Phys. Chem. Solids **4,** 241 (1958).

[35] T. Moriya, New Mechanism of Anisotropic Superexchange Interaction, Phys. Rev. Lett. **4,** 228 (1960).

[36] A. Fert and P. M. Levy, Role of Anisotropic Exchange Interactions in Determining the Properties of Spin-glasses, Phys. Rev. Lett. **44,** 1538 (1980).

[37] N. Nagaosa and Y. Tokura, Topological properties and dynamics of magnetic skyrmions, Nat. Nanotech. **8,** 899 (2013).

[38] L. Udvardi and L. Szunyogh, Chiral Asymmetry of the Spin-wave Spectra in Ultrathin Magnetic Films, Phys. Rev. Lett. **102,** 207204 (2009).

[39] K. Zakeri, Y. Zhang, J. Prokop, T.-H. Chuang, N. Sakr, W. X. Tang, and J. Kirschner, Asymmetric Spin-wave Dispersion on Fe(110): Direct Evidence of the Dzyaloshinskii-Moriya Interaction, Phys. Rev. Lett. **104,** 137203 (2010).

[40] A. T. Costa, R. B. Muniz, S. Lounis, A. B. Klautau, and D. L. Mills, Spin-orbit coupling and spin waves in ultrathin ferromagnets: The spin-wave Rashba effect, Phys. Rev. B **82,** 014428 (2010).

[41] D. Cortés-Ortuño and P. Landeros, Influence of the Dzyaloshinskii-Moriya interaction on the spin-wave spectra of thin films, J. Phys: Condens. Matter **25,** 156001 (2013).

[42] J.-H. Moon, S.-M. Seo, K.-J. Lee, K.-W. Kim, J. Ryu, H.-W. Lee, R. D. McMichael, and M. D. Stiles, Spin-wave propagation in the presence of interfacial Dzyaloshinskii-Moriya interaction, Phys. Rev. B **88,** 184404 (2013).

[43] K. Di, V. L. Zhang, H. S. Lim, S. C. Ng, M. H. Kuok, X. Qiu, and H. Yang, Asymmetric spin-wave dispersion due to Dzyaloshinskii-Moriya interaction in an ultrathin Pt/CoFeB film, Appl. Phys. Lett. **106,** 052403 (2015).

[44] K. Di, V. L. Zhang, H. S. Lim, S. C. Ng, M. H. Kuok, J. Yu, J. Yoon, X. Qiu, and H. Yang, Direct Observation of the Dzyaloshinskii-Moriya Interaction in a Pt/Co/Ni Film, Phys. Rev. Lett. **114,** 047201 (2015).

[45] V. L. Zhang, K. Di, H. S. Lim, S. C. Ng, M. H. Kuok, J. Yu, J. Yoon, X. Qiu, and H. Yang, In-plane angular dependence of the spin-wave nonreciprocity of an ultrathin film with Dzyaloshinskii-Moriya interaction, Appl. Phys. Lett. **107,** 022402 (2015).

[46] J. Cho, N.-H. Kim, S. Lee, J.-S. Kim, R. Lavrijsen, A. Solignac, Y. Yin, D.-S. Han, N. J. J. van Hoof, H. J. M.

Swagten, B. Koopmans, and C.-Y. You, Thickness dependence of the interfacial Dzyaloshinskii-Moriya interaction in inversion symmetry broken systems, Nat. Commun. **6,** 7635 (2015).

[47] H. T. Nembach, J. M. Shaw, M. Weiler, E. Jue, and T. J. Silva, Linear relation between Heisenberg exchange and interfacial Dzyaloshinskii-Moriya interaction in metal films, Nat. Phys. **11,** 825 (2015).

[48] M. Belmeguenai, J.-P. Adam, Y. Roussigné, S. Eimer, T. Devolder, J.-V. Kim, S. M. Cherif, A. Stashkevich, and A. Thiaville, Interfacial Dzyaloshinskii-Moriya interaction in perpendicularly magnetized Pt/Co/AlO$_x$ ultrathin films measured by Brillouin light spectroscopy, Phys. Rev. B **91,** 180405(R) (2015).

[49] A. A. Stashkevich, M. Belmeguenai, Y. Roussigné, S. M. Cherif, M. Kostylev, M. Gabor, D. Lacour, C. Tiusan, and M. Hehn, Experimental study of spin-wave dispersion in Py/Pt film structures in the presence of an interface Dzyaloshinskii-Moriya interaction, Phys. Rev. B **91,** 214409 (2015).

[50] N.-H. Kim, J. Jung, J. Cho, D.-S. Han, Y. Yin, J.-S. Kim, H. J. M. Swagten, and C.-Y. You, Interfacial Dzyaloshinskii-Moriya interaction, surface anisotropy energy, and spin pumping at spin orbit coupled Ir/Co interface, Appl. Phys. Lett. **108,** 142406 (2016).

[51] J. M. Lee, C. Jang, B.-C. Min, S.-W. Lee, K.-J. Lee, and J. Chang, All-electrical measurement of interfacial Dzyaloshinskii-Moriya interaction using collective spin-wave dynamics, Nano Lett. **16,** 62 (2016).

[52] S. Tacchi, R. E. Troncoso, M. Ahlberg, G. Gubbiotti, M. Madami, J. Åkerman, and P. Landeros, Interfacial Dzyaloshinskii-Moriya interaction in Pt/CoFeB films: Effect of the heavy-metal thickness, Phys. Rev. Lett. **118,** 147201 (2017).

[53] R. A. Gallardo, D. Cortés-Ortuño, T. Schneider, A. Roldán-Molina, F. Ma, R. E. Troncoso, K. Lenz, H. Fangohr, J. Lindner, and P. Landeros, Flat Bands, Indirect Gaps, and Unconventional Spin-wave Behavior Induced by a Periodic Dzyaloshinskii-Moriya Interaction, Phys. Rev. Lett. **122,** 067204 (2019).

[54] R. A. Gallardo, D. Cortés-Ortuño, R. E. Troncoso, and P. Landeros, *Three-dimensional Magnonics* (Jenny Stanford Publishing, Berlin, Heidelberg, 2019), p. 121.

[55] R. Verba, V. Tiberkevich, E. Bankowski, T. Meitzler, G. Melkov, and A. Slavin, Conditions for the spin wave nonreciprocity in an array of dipolarly coupled magnetic nanopillars, Appl. Phys. Lett. **103,** 082407 (2013).

[56] J. A. Otálora, M. Yan, H. Schultheiss, R. Hertel, and A. Kákay, Curvature-induced Asymmetric Spin-wave Dispersion, Phys. Rev. Lett. **117,** 227203 (2016).

[57] K. Di, S. X. Feng, S. N. Piramanayagam, V. L. Zhang, H. S. Lim, S. C. Ng, and M. H. Kuok, Enhancement of spin-wave nonreciprocity in magnonic crystals via synthetic antiferromagnetic coupling, Sci. Rep. **5,** 10153 (2015).

[58] M. Mruczkiewicz, P. Graczyk, P. Lupo, A. Adeyeye, G. Gubbiotti, and M. Krawczyk, Spin-wave nonreciprocity and magnonic band structure in a thin permalloy film induced by dynamical coupling with an array of Ni stripes, Phys. Rev. B **96,** 104411 (2017).

[59] S. Wintz, V. Tiberkevich, M. Weigand, J. Raabe, J. Lindner, A. Erbe, A. Slavin, and J. Fassbender, Magnetic vortex cores as tunable spin-wave emitters, Nat. Nanotechnol. **11,** 948 (2016).

[60] V. Sluka, T. Schneider, R. A. Gallardo, A. Kákay, M. Weigand, T. Warnatz, R. Mattheis, A. Roldán-Molina, P. Landeros, V. Tiberkevich, A. Slavin, G. Schütz, A. Erbe, A. Deac, J. Lindner, J. Raabe, J. Fassbender, and S. Wintz, Emission and propagation of 1D and 2D spin waves with nanoscale wavelengths in anisotropic spin textures, Nat. Nanotech. **14,** 328 (2019).

[61] M. N. Baibich, J. M. Broto, A. Fert, F. Nguyen Van Dau, F. Petroff, P. Etienne, G. Creuzet, A. Friederich, and J. Chazelas, Giant Magnetoresistance of (001)Fe/(001)Cr Magnetic Superlattices, Phys. Rev. Lett. **61,** 2472 (1988).

[62] A. Fert, Nobel lecture: Origin, development, and future of spintronics, Rev. Mod. Phys. **80,** 1517 (2008).

[63] P. A. Grünberg, Nobel lecture: From spin waves to giant magnetoresistance and beyond, Rev. Mod. Phys. **80,** 1531 (2008).

[64] P. Grünberg, Some ways to modify the spin-wave mode spectra of magnetic multilayers (invited), J. Appl. Phys. **57,** 3673 (1985).

[65] P. Grünberg, R. Schreiber, Y. Pang, M. B. Brodsky, and H. Sowers, Layered Magnetic Structures: Evidence for Antiferromagnetic Coupling of Fe Layers across Cr Interlayers, Phys. Rev. Lett. **57,** 2442 (1986).

[66] P. X. Zhang and W. Zinn, Spin-wave modes in antiparallel magnetized ferromagnetic double layers, Phys. Rev. B **35,** 5219 (1987).

[67] G. Binasch, P. Grünberg, F. Saurenbach, and W. Zinn, Enhanced magnetoresistance in layered magnetic structures with antiferromagnetic interlayer exchange, Phys. Rev. B **39,** 4828 (1989).

[68] M. Vohl, J. Barnaś, and P. Grünberg, Effect of interlayer exchange coupling on spin-wave spectra in magnetic double layers: Theory and experiment, Phys. Rev. B **39,** 12003 (1989).

[69] R. E. Camley and A. A. Maradudin, Magnetostatic interface waves in ferromagnets, Solid State Commun. **41,** 585 (1982).

[70] K. Mika and P. Grünberg, Dipolar spin-wave modes of a ferromagnetic multilayer with alternating directions of magnetization, Phys. Rev. B **31,** 4465 (1985).

[71] P. Grünberg and K. Mika, Magnetostatic spin-wave modes of a ferromagnetic multilayer, Phys. Rev. B **27,** 2955 (1983).

[72] R. L. Stamps and R. E. Camley, Magnetostatic modes in thin film antiferromagnet/ferromagnet layered systems, J. Magn. Magn. Mater. **54,** 803 (1986).

[73] J. Barnaś and P. Grünberg, Spin waves in exchange-coupled epitaxial double-layers, J. Magn. Magn. Mater. **82,** 186 (1989).

[74] N. R. Bernier, L. D. Tóth, A. Koottandavida, M. A. Ioannou, D. Malz, A. Nunnenkamp, A. K. Feofanov, and T. J. Kippenberg, Nonreciprocal reconfigurable microwave optomechanical circuit, Nat. Commun. **8,** 604 (2017).

[75] Z. Shen, Y.-L. Zhang, Y. Chen, F.-W. Sun, X.-B. Zou, G.-C. Guo, C.-L. Zou, and C.-H. Dong, Reconfigurable optomechanical circulator and directional amplifier, Nat. Commun. **9,** 1797 (2018).

[76] See Supplemental Material at http://link.aps.org/supple mental/10.1103/PhysRevApplied.12.034012 for a brief description of the theoretical and experimental techniques used in the paper, which includes Refs. [82] and [83].

[77] J.-V. Kim, R. L. Stamps, and R. E. Camley, Spin Wave Power Flow and Caustics in Ultrathin Ferromagnets with the Dzyaloshinskii-Moriya Interaction, Phys. Rev. Lett. **117**, 197204 (2016).

[78] A. Vansteenkiste, J. Leliaert, M. Dvornik, M. Helsen, F. Garcia-Sanchez, and B. Van Waeyenberge, The design and verification of MuMax3, AIP Adv. **4**, 107133 (2014).

[79] A. K. Chaurasiya, C. Banerjee, S. Pan, S. Sahoo, S. Choud-hury, J. Sinha, and A. Barman, Direct observation of inter-facial Dzyaloshinskii-Moriya interaction from asymmetric spin-wave propagation in $W/CoFeB/SiO_2$ heterostructures down to sub-nanometer CoFeB thickness, Sci. Rep. **6**, 32592 (2016).

[80] A. K. Chaurasiya, S. Choudhury, J. Sinha, and A. Bar-man, Dependence of Interfacial Dzyaloshinskii-Moriya Interaction on Layer Thicknesses in $Ta/CoFeB/TaO_x$ Heterostructures from Brillouin Light Scattering, Phys. Rev. Appl. **9**, 014008 (2018).

[81] R. Mock, B. Hillebrands, and R. Sandercock, Construction and performance of a Brillouin scattering set-up using a triple-pass tandem Fabry-Perot interferometer, J. Phys. E: Sci. Instrum. **20**, 656 (1987).

[82] S. Y. Jang, S. H. Lim, and S. R. Lee, Magnetic dead layer in amorphous CoFeB layers with various top and bottom structures, J. Appl. Phys. **107**, 09C707 (2010).

[83] H. T. Nembach, T. J. Silva, J. M. Shaw, M. L. Schneider, M. J. Carey, S. Maat, and J. R. Childress, Perpendicular fer-romagnetic resonance measurements of damping and Landé g–factor in sputtered $(Co_2Mn)_{1-x}Ge_x$ thin films, Phys. Rev. B **84**, 054424 (2011).